IOP Publishing Mater. Quantum Technol. 3 (2023) 043001 https://doi.org/10.1088/2633-4356/ad13a0

Materials for Quantum Technology

OPEN ACCESS

RECEIVED
24 April 2023

REVISED
26 September 2023

ACCEPTED FOR PUBLICATION
8 December 2023

PUBLISHED
20 December 2023

PERSPECTIVE

Singly doped colloidal quantum dots as optically addressed nanopositionable qubits

Rachel M Barrett and David J Binks*

Department of Physics and Astronomy & Photon Science Institute, University of Manchester, Manchester M13 9PL, United Kingdom
* Author to whom any correspondence should be addressed.

E-mail: david.binks@manchester.ac.uk

Keywords: spin qubit, colloidal quantum dot, spin-photon interface

Abstract

Colloidal quantum dots (CQDs) are isolated semiconductor nanocrystals with a size-tunable bandgap that can be prepared and processed by well-established solvent-based chemistry, and are currently used for a number of optoelectronic applications. When doped with a single atom, they also have great potential as a platform for optically addressable spin qubits. This perspective first describes the process by which doped CQDs can be made and the electronic structure produced in them by doping with a single atom. The properties that make them particularly well-suited as a spin-photon interface are identified: a local environment for the dopant that is free of unwanted spins; an optical cross-section for the dopant that can be enhanced by orders of magnitude via an exchange interaction with the band edge exciton of the dot; and, as an isolated nanocrystal, the scope for nano-positioning and hence precise incorporation into device structures. Lastly, two areas for development are discussed which would enhance the impact of singly doped quantum dots on quantum technology. The first of these is a synthetic method that ensures deterministic doping with single atoms and the second is to expand the range of dopants available.

1. Introduction

Colloidal quantum dots (CQDs) are semiconductor nanocrystals that are small enough to confine carrier wave-functions, resulting in a size-tunable bandgap -see figure 1. A wide range of CQD compositions and structures can be fabricated using low-cost, solvent-based methods and then processed into device structures. First synthesised in the 1980s [1, 2], CQDs have been developed over the intervening decades into a mature, well-understood material system that benefits from a suite of facile and scalable synthesis and processing techniques [3]. Today, as well as still being the subject of an active research effort world-wide, CQDs are manufactured commercially by several companies across the globe and used for numerous real-world applications. Specialist CQD manufacturers include Nanoco Technologies Ltd in the UK; Nexdot in France; QD Laser of Japan; and Nanosys, Ocean NanoTech, NN-Labs in the USA, amongst others. The range of applications for which CQDs have been used include solar cells [4], photodetectors [5], light-emitting diodes [6], lasers [7], biological sensing and imaging [8], and display technology [9].

CQDs have also been studied as a promising materials platform for quantum technologies, with the work in this area recently reviewed [10]. Their discrete energy levels, near-unity photoluminescence (PL) quantum yields (QY) [11], and the facile routes by which they can be synthesised, and the ease, as isolated nanocrystals, with which they can be integrated into an optical cavity has motivated investigators to study their properties as coherent single photon emitters. Single photon emission (SPE) from undoped CQDs was first reported over 20 years ago [12] and subsequently a $g^{(2)}(0)$ value, which characterises the single-photon purity, as good as <0.01 for optical excitation at room temperature has been reported [13]. SPE with $g^{(2)}(0) < 0.05$ has been demonstrated for electrical excitation, also at room temperature [14]. However, the optical coherence time, T_2, of CQDs is typically reduced by strong-electron phonon coupling [15], spectral diffusion [16] and PL 'blinking' [17]. For quantum information applications, T_2 should ideally be twice the emission lifetime, T_1. The shortened T_2 of most CQD types compared to their T_1 has thus far limited their

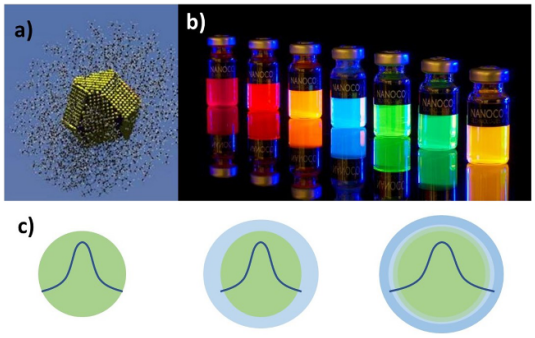

Figure 1. (a) Model of a CQD showing a CdTe nanocrystal with organic surface ligands. Reproduced from [11]. CC BY 4.0. (b) Dispersions of CQDs of different diameters showing size-tunability of the band gap (© Nanoco Technologies Ltd). (c) Carrier wavefunction (blue line) in a core-only CQD (left), core–shell CQD (middle), and core graded shell CQD.

use for SPE. The best $T_2/2T_1$ ratio has been demonstrated for perovskite CQDs which, at ∼0.2, is similar to those achieved for epitaxial quantum dots [18]; in this case however, the utility of these CQDs is restricted instead by their instability under ambient conditions.

Doping with impurities, particularly transition metals (TMs) and rare earths (REs), has also been extensively studied, with a view to controlling the optical [19] and electronic [20] properties of the CQDs. Attempts at doping were initially hindered by unforeseen difficulties in incorporating impurity atoms within the CQD, an effect sometimes described as 'self-purification'; however, these difficulties were eventually overcome with a greater understanding of the process of impurity adsorption to the growing CQD core [21]. CQDs can also be doped post-growth via cation exchange [22] or intentional exposure of the CQD surface to the desired dopant, resulting in incorporation [23]. Individual CQDs doped by single impurity atoms have been produced and studied, motivated by their magneto-optic properties and potential use in spintronic applications [24]. However, this has typically been achieved by reducing the concentration of the impurity during synthesis so that on *average* there is approximately one dopant atom per CQD, and then the resulting population is searched until an example of a singly doped CQD is found [25].

This perspective will describe the outstanding potential of CQDs doped with single atoms as a platform for optically addressed spin-qubits. Applications of such qubits include as the basis of a quantum memory that can be used to extend the range of quantum communications or enable distributed quantum computing [26]. It will outline the well-established synthetic and processing techniques, developed over more than 30 years, that enable CQDs of a wide range of compositions, including doped CQDs, to be produced with near-atomic precision and then assembled into device structures with nanoscale accuracy. The electronic structure of doped CQDs, which will be the basis of the proposed spin-qubits will then be described. The properties of doped CQDs that make them particularly well-suited as a host materials system for optically addressable spin-qubits will be discussed. Lastly, the next steps in the development of CQD-based spin qubits will be identified.

2. Synthesis and electronic structure

2.1. Outline of techniques for CQD synthesis

CQDs may be synthesised in the gas-phase [27], whereby precursors are decomposed into their constituent ions and atoms, for example using a furnace [28] or plasma [29]; nanocrystals then form upon subsequent cooling and are bubbled through a solvent to create a colloidal dispersion. Wet-chemical synthesis of CQDs may also be achieved via aqueous arrested precipitation techniques, whereby metal salt precursors are added to an aqueous solution; a dynamic equilibrium is established which favours precipitation due to the low aqueous solubility of binary semiconductor alloys [30, 31]. The colloidal stability may then be improved by the post-synthesis attachment of organic ligands [32].

Alternatively, monodisperse CQDs can be prepared by creating a supersaturation of 'monomers' in a process known as solvothermal synthesis [33]. The term monomer here refers to the smallest semiconductor subunit, consisting of an anion and cation; monomer species may be produced via, for example, 'hot injection' [34], whereby the precursors are reacted at high temperature. The monomer concentration rapidly reaches supersaturation and is then relieved by nucleation. Once the monomer concentration drops below the threshold for the formation of new nuclei, further growth occurs on the existing nuclei; the size of the nanocrystals may be tuned by varying the precursor concentration, allowing a narrow size distribution to be obtained [35].

Once the size of the CQDs increases above a critical size at which the monomer concentration at the surface of the CQD becomes equal to the bulk concentration in the solution, a growth stage known as Ostwald ripening [36] is entered. CQDs larger than this critical size grow at the expense of smaller CQDs and thus the average size of the distribution increases over time [35].

Because CQDs have high surface-to-volume ratios, trap states localised at the surface can have a significant impact on their optical properties [37]. Unbound surface atoms form sites that dissociate excitons, thereby reducing excitonic emission; for example, in CdSe, undercoordinated Cd atoms act as electron traps while dangling Se bonds act as hole traps [36, 38]. These surface traps may be passivated by the post-synthesis attachment of organic ligands; as well as stabilising the dispersion of CQDs in solution, ligand coating minimises the number of surface atoms with reduced coordination number [39]. However, the passivation of surface trap states by ligands has been shown [37, 40] to be incomplete. The spins of non-passivated dangling bonds of surface ions can interact with the exciton, for example to provide a spin-flip assisted radiative recombination pathway from dark excitonic states [41]; the formation of dangling bond magnetic polarons may explain the observation of magnetic properties for non-magnetic CQDs [42].

Surface trap states may also be passivated by the growth of inorganic ligand shells around the CQD- see figure 1(c). Shells may be grown one monolayer at a time via alternating injection of cationic and anionic precursors [43], allowing precise control over shell thickness. In addition to surface trap passivation, surrounding the CQD core with a shell made of an alloy with a wider bandgap increases the quantum confinement of excitons in the core [44] and enhances the PLQY [45].

The mismatch in bond length between the core and shell materials can, however, generate strain. For large CQDs, there exists a critical shell thickness above which lattice defects may form at the core–shell interface to ease the strain, introducing carrier traps [46]. For small CQDs, the strain may be tolerated, and the deformation forces the materials to adopt unnatural bond lengths, which alters the electronic bandgap; for example, in II–VI and III–V materials, compressive strain widens the bandgap [43]. The lattice strain can be reduced by softening the steepness of the interface between core and shell materials by growing an alloy shell with a compositional gradient [47]. For example, high fluorescence QYs (70%–85%) have been reported for CdSe-core CdS/ZnCdS/ZnS multishell CQDs [48].

2.2. Doping techniques

The properties of CQDs may be tuned by doping with impurity atoms. This may be achieved by adding impurity precursors during the hot-injection process [49] or via cation exchange, whereby metal salts in solutions are mixed with solutions of preformed CQDs [50]. Incorporating dopant atoms into the host lattice can, however, be challenging: the reaction temperature must be carefully controlled, since the CQD diameter is comparable to the mean free path of ion diffusion through the lattice [51] which can lead to the expulsion of impurities in a 'self-purification' [52] effect; the adsorption of impurity atoms onto the CQD surface during growth is also impacted by the surface morphology and the surfactants in the growth solution [21]. The number of impurity ions successfully incorporated per CQD in this way follows a Poisson distribution. Multiple dopants confined within a single CQD will interact with each other due to the small CQD volume; this has a significant effect on electronic structure [47].

2.3. Electronic structure of doped CQDs

The conduction and valance bands of a semiconductor nanocrystal split into discrete energy levels as its size becomes similar to or smaller than the Bohr radius, $\boldsymbol{a_{e,h}}$ of the carriers, where

$$\boldsymbol{a_{e,h}} = \frac{\hbar^2 \varepsilon_\infty}{\boldsymbol{m_{e,h}^2 e^2}} \tag{1}$$

and $\boldsymbol{m_{e,h}}$ is the effective mass of electron/hole, ε_∞ is the static dielectric constant for the semiconductor. The electron levels are labelled nL_e, where $n = 1,2,3\ldots$ is the radial quantum number, and the orbital quantum numbers, $L = 0,1,2,3\ldots$ correspond to the labels S, P, D and F, respectively, in spdf notation; the lowest energy electron state is $1S_e$. The hole states can either be labelled in a similar way i.e. nL_h, or, to describe their more complex substructure, the hole states can instead be labelled nL_F, where $F = J + L$ is the total angular momentum and J is the Bloch-function angular momentum; the lowest energy hole state is $1S_{3/2}$ [53].

The electronic levels associated with a dopant in a CQD can be classed as either shallow or deep depending on whether they are close enough to the electron and holes states of the CQD to allow thermal excitation at operating temperatures. The electronic states of a shallow dopant can be treated as donor or acceptor levels within the host semiconductor, whilst those of a deep dopant are instead described by molecular orbit theory. Here, the energy levels are described by molecular symmetry notation, in which letters (lower and upper case for single and multi-particle states, respectively) and subscripts represent the

corresponding point group and indicate the symmetry of the orbital; a superscript is used to indicate the degeneracy of the state [10]. For Mn^{2+} in a ZnS CQD for example, the degeneracy of the half-filled 3d level of the Mn^{2+} is broken by the crystal field resulting in a $^6A_1$ ground state and a $^4T_1$ excited state.

Importantly, there can be a significant magnetic-exchange coupling between unpaired spins on the dopant and the unpaired spins on the carriers comprising a photogenerated exciton in the CQD, which can be exploited to optically probe and control the dopant spin state. For example, in prototypical Mn^{2+} doped CQDs this coupling can be described by a ferromagnetic *s–d* interaction between the conduction band electron and dopant and a net antiferromagnetic *p–d* interaction between the hole and dopant [54]. Crucially, these exchange interactions occur even without an applied magnetic field, enabling light-induced spin polarisation in CQDs containing multiple dopants [55] and giant zero-field energy level splitting, $\boldsymbol{\Delta E_{e,h}}$ in singly-doped CQDs [56]; as detailed below, this latter effect enables the optical control of spin states and qubits. The magnitude of the splitting for the electron can be expressed as [56]

$$\boldsymbol{\Delta E_e = 205\,|\alpha|\,V_0 \Psi_e^2(R)} \tag{2}$$

where $\boldsymbol{V_0}$ is the volume of the unit cell, $|\boldsymbol{\alpha}|$ is the average value of the exchange integral for the electron and $\boldsymbol{\Psi_e(R)}$ is the electron wavefunction at the position of the dopant, $\boldsymbol{R}$. The value of $\boldsymbol{\Psi_e^2(R)}$ is maximised when the dopant is located in the CQD centre and zero when it is at the dopant surface; a dopant located at a random distance from the CQD centre results, on average, in a $\boldsymbol{\Delta E_e}$ value that is 6 times smaller than when the dopant is at the CQD centre [56]. $\boldsymbol{\Delta E_e}$ also increases linearly with the inverse CQD volume, as a reduced size also enhances $\boldsymbol{\Psi_e^2(R)}$. The corresponding expression for $\boldsymbol{\Delta E_h}$ is more complex but is also maximised for a centrally located dopant and increases with decreasing CQD volume [56]. Thus, the zero-field energy level splitting that can be used for optical control of the Mn^{2+} states is maximised for CQDs of small size and with dopants located as close as possible to the centres. The value of $\boldsymbol{\Delta E_{e,h}}$ can also be tuned using the scope for wave-function engineering afforded by a core/shell CQD structure. Bussian *et al* [57] showed the Zeeman energy splitting could be tuned from about −14 meV to +7 meV by increasing the thickness of a CdSe shell surrounding a Mn^{2+}-doped ZnSe core, which localises the hole in the shell away from dopant and so reduces $\boldsymbol{\Delta E_h}$ relative to $\boldsymbol{\Delta E_e}$. Significant exchange interactions have also been demonstrated for other TM dopants, such as Cu^{2+} [58], Co^{2+} [59] and Cr^{2+} [60].

The exchange interaction between the confined carriers and the magnetic dopant depends on the filling of the 3*d* orbital of the dopant atom. For example, in II–VI semiconductors, Cr incorporates as Cr^{2+} with non-zero orbital angular momentum $L = 2$. This modifies the crystal field and spin–orbit coupling, resulting in a spin to strain coupling [60] much larger than for systems with dopants without orbital angular momentum, such as Mn-doped II–VI semiconductors [61]. This large spin to strain coupling may be of use in hybrid spin-mechanical system applications [62], in which an individual spin qubit is coupled to a mechanical oscillator.

2.4. Probing and controlling dopant spins and qubits

Successful incorporation of dopant ions into the CQDs can be demonstrated by electron spin resonance (ESR) experiments, with six characteristic peaks in the ESR spectrum being the signature for exchange splitting in Mn^{2+} (see section 3.2). If the concentration of Mn^{2+} is low ($\lesssim$0.1%), these peaks appear sharp; however, at higher dopant concentrations, the width increases [63], likely due to the increased likelihood of dipolar interactions between neighbouring Mn^{2+} ions [64]. In contrast, for CQDs doped with Cu^{2+}, which has non-zero orbital angular momentum, strong spin–orbit and Jan–Teller coupling can broaden electron paramagnetic resonance (EPR) lines, making them too weak to be observable [65].

Magnetic circular dichroism (MCD), which compares the absorption of left and right-hand circularly polarised light as a function of applied magnetic field, $\boldsymbol{B}$, can be used to investigate the Zeeman splitting, $\boldsymbol{\Delta E_Z}$, produced by the exchange interaction between the exciton and dopant [56, 57, 66]. This splitting can be described by [24]

$$\boldsymbol{\Delta E_Z = g_{int}\mu_B B + \Delta E_{sp-d}^{avg}(\langle S_z\rangle)} \tag{3}$$

where $\boldsymbol{g_{int}}$ is the intrinsic *g*-factor for the exciton, $\boldsymbol{\mu_B}$ is the Bohr magneton, and $\boldsymbol{\Delta E_{sp-d}^{avg}}$ is the contribution to the MCD signal due to the exchange interaction averaged over the CQDs in the sample. This average depends not only the average CQD size and dopant location but also on the spin expectation value, $\langle \boldsymbol{S_z}\rangle$, along the direction of $\boldsymbol{B}$, which depends on both the temperature, $\boldsymbol{T}$, and the magnitude of $\boldsymbol{B}$ and can be described by:

$$\boldsymbol{\langle S_z\rangle = -\frac{1}{2}\left[(2S+1)\,coth\left((2S+1)\,x\right) - coth\,(x)\right]} \tag{4}$$

where $x = g_{dop}\mu_B B/2kT_{eff}$, S is the total spin of the dopant (e.g. $S = 5/2$ for Mn^{2+}), g_{dop} is the g-factor for the dopant ion and T_{eff} is the sum of T and the antiferromagnetic temperature, T_{AF}, which was introduced to allow for the effect of antiferromagnetic interaction between dopants [67]. The sign of g_{dop} and thus of ΔE_Z differs depending on the dopant species; for example, ΔE_Z has a positive sign in Cu^{2+}-doped ZnSe CQDs [58], while a negative ΔE_Z is observed for Mn^{2+}:ZnSe [59, 68] and Co^{2+}:CdSe CQDs [59]. This technique provides information on the effective g-factor, g_{eff}, which is the sum of g_{int} and the g-factor induced by sp–d exchange in the doped CQDs, and thereby on the strength of the exchange interaction between the dopant and exciton. For instance, $|g_{eff}|$ values in excess of 200 have been reported for Mn^{2+} doped CQDs, which are ∼100-fold greater than values for equivalent undoped CQDs.

Not all magnetic dopants necessarily contribute fully to the magnetisation measured for magnetically doped CQDs. For example, nearest neighbour Mn^{2+}-Mn^{2+} dimer pairs couple antiferromagnetically in II–VI and III–V CQDs and are thus magnetically silent. Dimer formation reduces the effective concentration of Mn^{2+} participating in exchange interactions and is therefore typically detrimental in magneto-optical and magnetoelectronics applications [69]. However, in charged nanocrystals, conduction band electrons have been shown to mediate exchange interactions between dimer pairs and distant Mn^{2+} ions, eliminating the antiferromagnetic coupling [70]; the magnetic properties of CQDs can thus be controlled via manipulation of their charge states [71].

The capability to optically manipulate ensembles of dopant spins is important for spin-photonics [72], which may be achieved by utilising the magnetic exchange interactions described above. When a QD is photoexcited, the spins of the magnetic dopants may align under the effective magnetic field of the confined exciton, forming an excitonic magnetic polaron (EMP) [73]. EMPs are enhanced by exciton spatial localisation [62] and so form more readily in CQDs as opposed to in epitaxially grown QDs, for which exciton confinement is weaker [74]. For CQDs doped with Mn^{2+}, energy transfer to Mn^{2+} after photoexcitation is faster than the reorientation of the dopant spins, hindering EMP formation; however, if the CQDs are prepared such that their excitonic energy levels lie below all Mn^{2+} excited states, this transfer is eliminated, enabling the detection of complete magnetisation at temperatures up to 50 K in CdSe CQDs, with signatures of photomagnetisation observable even at room temperature [55]. The magnetic response of doped CQDs may also be tuned optically; for example, it has been demonstrated that following illumination with UV light, Cu-doped ZnSe–CdSe core–shell CQDs exhibit pronounced photoinduced paramagnetisation, persisting for hours in the dark [58]. This long-lived photoinduced magnetisation suggests that Cu-doped CQDs may be of particular use in magneto-optical data storage applications.

The dynamics of isolated spins are key to the properties of singly doped quantum dots. The spin-flip rate for Mn^{2+} in CdTe self-assembled quantum dots has been measured to be ∼20 ns by both photon correlation [75] and resonant optical pumping methods [76]. The spin state of single dopants in single quantum dots can also be initialised, manipulated and readout by optical techniques. A scheme for the optical pumping of the spin states in single Mn^{2+} doped self-assembled CdTe/ZnTe quantum dots was proposed in 2005 [77], with further modelling showing that a single Mn^{2+} could be prepared into any of its 6 spins states by a sequence of ultrafast pulses tuned to be resonant with either its light hole or heavy hole excitonic transition [78]. The transition between spins-states could be achieved with single optical pulses under a large applied magnetic field of $B = 9$ T but even under zero field it could be achieved with ∼5 pulses and completed in a few 10 s of ps. The Mn^{2+} spin-state thus prepared remains after removal of the excitons for a period characterised by the spin-flip lifetime and can be readout optically within this period by absorption or PL excitation measurements. The experimental control of Mn^{2+} spin-states in a self-assembled CdTe quantum dot using resonant optical excitation was later demonstrated using nanosecond laser pulses, with preparation into a particular state achieved with 75% efficiency and taking a few tens of nanoseconds, with state readout via subsequent circular polarisation- and frequency-resolved PL [76].

The preparation of spin-qubit in a Mn^{2+} doped dot can be achieved optically via the following steps [77]: non-resonant excitation followed by detection of a left-hand circularly polarised (σ^+) photon emission at an energy corresponding to a transition to the Mn^{2+} +5/2 spin state; from this initial state, a resonant circularly polarised laser pulse then generates a qubit involving the +5/2 and −5/2 spin states. Once spin-photon entanglement has been generated locally in separate CQDs then the two photonics modes can be interfered at a beam-splitter, erasing the which-path information. Subsequent photon detection heralds the generation of spin-spin entanglement between the two CQDs.

The spin properties of dopants may also be controlled electrically. For example, magnetic polarons may be electrically induced by current injection into Mn^{2+}-doped CdSe QDs embedded in the active layer of light emitting devices [79], and the spin configuration of a single Mn dopant within a CdTe QD may be tuned by altering the charge state of the QD [80].

Table 1. Comparison of spin coherence lifetimes for example optically-addressable qubits.

Material system	Spin coherence lifetime	References
Mn:PbS CQDs	8 μs	Moro *et al* [81]
Perovskite CQDs	78 ps	Utzat *et al* [18]
NV in nanodiamonds	400 μs	Wood *et al* [82]
NV in diamond	14.3 ms	Bernien *et al* [83]
SiV in diamond	13 ms	Sukachev *et al* [84]
InGaAs self-assembled QDs	1.7 μs	Stockill *et al* [85]
SiV in SiC	0.85 ms	Nagy *et al* [86]
Er^{3+} in Y_2SiO_5	3.3 μs	Raha *et al* [87]

3. The case for singly doped CQDs as a spin qubit platform

3.1. A 'material vacuum'

The coherence lifetime of a spin-based qubit depends on its environment since interactions with defects, impurities and nuclear spins in its vicinity tend to cause it to decohere. Ideally, the spin qubit would be placed in a vacuum but in most realisations, it is instead embedded in a material system. A good host system for the qubit should thus by a 'material vacuum' i.e. one which is sufficiently free of the sources of such interactions so that the coherence lifetime remains long enough for the intended application. The spin coherence lifetimes of a number of example optically-addressable qubits are compared in table 1, including doped CQDs. Most of the examples selected are hosted in a solid-state host material since these are most suitable for on-chip integration. However, an atomic vapour-based platform has also been included for comparison since this is being actively developed for commercial applications. As table 1 shows the spin coherence lifetimes, which determine the qubit lifetime, for these examples range from a few μs to as much as 14.3 ms for nitrogen vacancies in bulk diamond, although this drops significantly for the nanodiamonds that are the most suitable for on-chip integration. It is worth noting that the lifetimes shown are for electronic spins and that, as discussed below, much longer qubit lifetimes can be achieved by coupling to the nuclear spins in some systems.

As shown in table 1, a spin coherence lifetime of 8 μs has been reported for core-only, randomly-doped Mn^{2+}:PbS_CQDs. However, using the suite of synthetic growth established for CQDs, it is possible to engineer CQDs with improved spin coherence lifetimes. The self-purification process that can result in the expulsion of impurities from the CQD, and which initially hindered attempts at doping, tends to expel other types of defects as well [88]. The defects and impurities that might thus interact with a dopant-based spin-qubit embedded in a CQD are thus largely found on its surface. These can also produce non-radiative recombination pathways and so several techniques have been refined over the years to isolate an exciton in the CQD core from the surface and thus increase the PL QY [89]. However, they can be re-purposed to isolate a spin qubit located within the CQD core from defects and impurities on the surface. In particular, the growth of a thick shell layer composed of a wide bandgap material around the core can act as a potential barrier so that the wavefunction of an exciton in the core does not significantly overlap with spins on the surface. As described in section 2.1, originally the shell of a different material was simply grown on the surface but the abrupt compositional change that this produced was found to result in defects at the interface due to the lattice mismatch. However, the development of techniques to grow CQDs with a graded compositional change from core to shell significantly reduced this effect resulting in PL QY values of, for instance, 85% in CdSeS CQDs [90]. Moreover, an ESR study [91] on the effect of adding an undoped CdSe shell onto a CdSe core doped with Mn^{2+} found that a shell thickness of only 1 nm was sufficient to make the effect on the Mn^{2+} of nuclear spins on the CQD surface negligible—see figure 2. This sensitivity to the separation, r, between dopant and surface is attributed to the interaction between them being mediated by dipole–dipole coupling, which has a $1/r^6$ dependence (after averaging over possible Boltzmann-weighted orientations). This result indicates that if the dopant can be reliably located in the centre of CQD core that is more than 2–3 nm thick then a shell layer may not be necessary to effectively isolate it from spins located on the surface.

The same study also reported features in the ESR spectra indicating an interaction between the Mn^{2+} and nearby atoms of Cd and Se which were isotopes with non-zero nuclear spin. A further advantage of CQDs as host systems for spin qubits is that they can be fabricated from elements with a high fractional abundance of spin-0 isotopes. For instance, ZnS CQDs are long-established [93] and naturally occurring Zn and S are composed of 96% and 99% spin-0 isotopes, respectively. Isotopically selected precursor species of these elements could be used to control the abundance of nuclear spins in the CQD further. This control might be exercised to reduce the nuclear spin bath to zero to maximise the lifetime of spin on the dopant. Alternatively, the presence of a nearby nuclear spin to which the electron spin on the dopant can couple

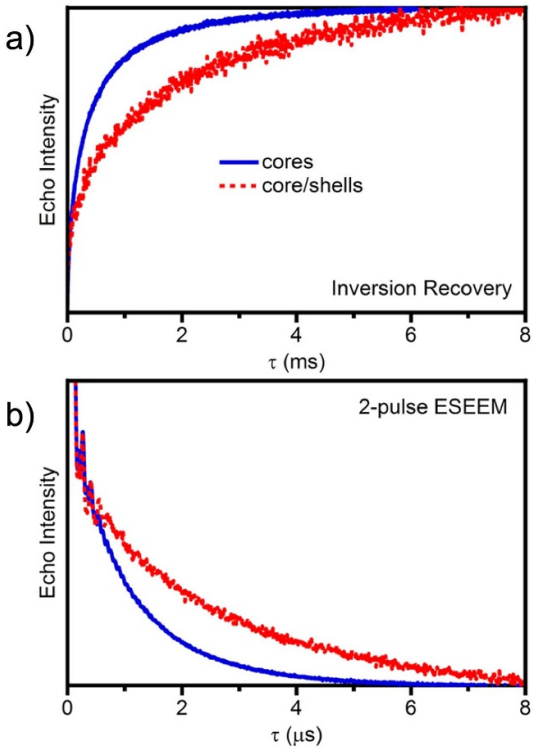

Figure 2. Comparison of the EPR response of Mn^{2+} doped CQDs with and with a shell layer that isolates the dopant in the core from the surface. (a) The spin-lattice relaxation time is measured by an inversion recovery technique, whilst (b) the spin coherence lifetime is determined by a 2-pulse electron spin echo envelope modulation (ESEEM) method. Reprinted (adapted) with permission from [91]. Copyright (2015) American Chemical Society.

provides the possibility of a long-term quantum memory, analogous to a nitrogen-vacancy (NV) qubit coupled to a ^{13}C nuclear spin in diamond for which coherence times >1 s have been demonstrated [92].

3.2. Enhanced optical cross-section

Single transition metal (TM) and rare-earth (RE) dopants are well suited as the host for spin-qubits since they possess optically addressable transitions within their open *d*- and *f*-shells, respectively. These orbitals are not typically involved in bonding and so are less sensitive to their environments. Transitions with these shells are both spin- and parity-forbidden, becoming only weakly allowed in a crystalline host due to spin–orbit coupling and the low symmetry of the crystal field at the dopant, resulting in long (μs to ms) lifetimes. Further, for RE dopants the *f*-shell is shielded from its environment to a significant degree by the outer orbitals so that lifetimes are increased compared to TM dopants. Such extended lifetimes can be beneficial to an optically generated spin-state since radiative recombination is the ultimate limit on its duration. However, the low dipole moments of these states, typically 0.001–0.1 Debye (*D*) [10], that result in their long lifetimes also means that they have small optical cross-sections, which makes it very challenging to efficiently couple single photons to individual dopants. This issue can be addressed to some extent using high finesse optical micro-cavities to increase the coupling efficiency, and such approaches have resulted in the successful optical addressing of single dopants, including REs [94, 95].

Embedding TM or RE dopants in CQDs provides a potential route to enhancing the optical cross-section of spin-qubits. The dipole moment of typical QDs ranges from ~40 to 100 *D* [98] i.e. 3–5 orders of magnitude greater than the values for individual TM and RE dopants. Coupling the band edge excitonic transition of the CQD with the spin-state of the dopant affords a way by which the optical cross-section of the qubit on the dopant can be significantly improved. Studies on Mn^{2+}-doped CQDs have investigated this coupling and its dependence on CQD size and structure, which is a result of an exchange interaction between band edge carriers and the dopant. The consequence of this coupling depends on the size of the CQD band gap relative to the optical transition on the Mn^{2+}. For smaller CQDs whose band gap is significantly larger than the $^6A_1$–$^4T_1$ Mn^{2+} transition, the band edge excitation of the CQD is transferred to the Mn^{2+} on a picosecond timescale, resulting in emission from the dopant [99–101]—see figure 3(a). This emission can be spin-polarised but unfortunately its polarisation was found to be independent of the polarisation of the exciting photon [102] making it unsuitable as an optically addressable qubit. However, for larger CQDs with bandgap less than the Mn^{2+} transition energy, the excitation remains as a band edge CQD exciton, but its

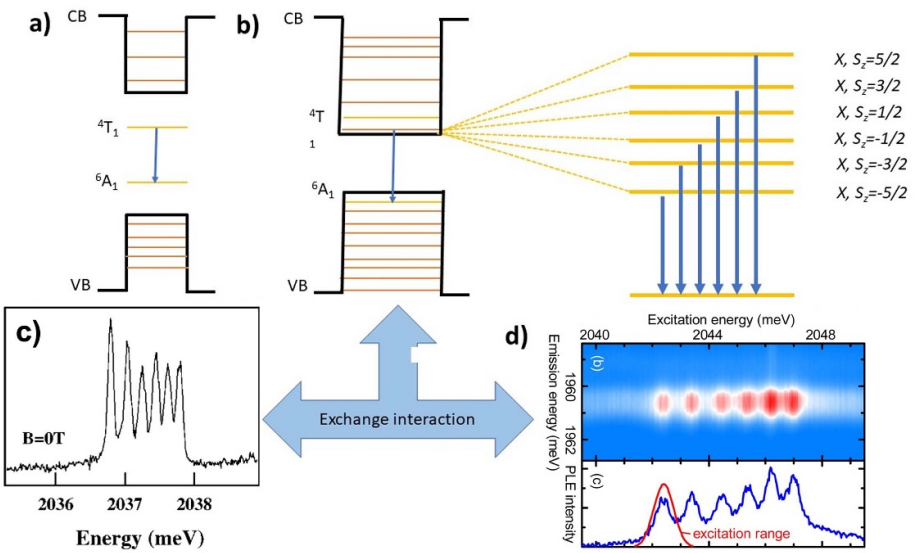

Figure 3. (a) For CQDs with a bandgap greater in energy than the $^4T_1$ to $^6A_1$ transition in Mn^{2+}, the emission is from the dopant. (b). When the bandgap energy is less than this transition, an exchange interaction with the dopant modifies the exciton into 6 spin-dependent states. Work on similar self-assembled Mn^{2+}:CdSe QDs has shown that the 6 states (c) emit independently, and (d) can be individually addressed by control of the energy and polarisation of the exciton photon. (c) Reprinted figure with permission from [96], Copyright (2004) by the American Physical Society. (d) Reprinted figure with permission from [97], Copyright (2014) by the American Physical Society.

electronic structure is modified, via the exchange interaction, by the spin-state of the $^6A_1$ level of the Mn^{2+}. In particular, the exciton is split into sub-levels corresponding to the 6 possible projections of the $S = 5/2$ $^6A_1$ Mn^{2+} ground level—see figure 3(b); moreover, the energy difference between these sub-levels is significant even at zero applied magnetic field and depends on the location of the dopant within the CQD. These states emit individually [25, 96] and work on similar self-assembled quantum dots has shown that the states can be optically addressed [97] by control of the energy and/or polarisation of the exciting photon [103], enabling optical initialisation and readout of the spin state [76]—see figures 3(c) and (d). Naturally occurring manganese contains just one isotope, [54] Mn, which has a 5/2 nuclear spin enabling the transfer of electron spin to nuclear spin for longer term storage. Successful mapping of the electron spin state to the surrounding ensemble of nuclear spins via the hyperfine interaction has already been demonstrated in self-assembled QDs [104, 105], enabling spin information to be stored for up to milliseconds [106], suggesting that it should also be possible for CQDs.

3.3. Nano-positioning

An important advantage of doped CQDs is that they are formed as a colloidal dispersion of individual nanocrystals. This colloidal form has allowed an extensive library of solution-based techniques to be developed that enables the integration of CQDs into device structures [107]. Of relevance to the development of a platform for optically addressed qubits is the ability to isolate a single nanocrystal and position it into an optical micro-cavity or nanoantenna to increase the coupling efficiency of the spin qubit with photons. Here, the ∼5–20 nm typical size of the CQDs is useful: large enough to be manipulated, as described below, but small enough so that they can be located entirely at the focus of an optical micro-cavity or nano-antenna, ensuring that the dopant that they host is ideally positioned wherever it is within the CQD.

Much of the work on positioning nanocrystals reported to date has focused on nano-diamonds since they host NV centres, which are well-established as optically- addressable spin qubits, although the techniques are suitable for other types of nanocrystals. In particular, 'pick and place' techniques have been developed that the use the tip of atomic force microscope (AFM) to move individual nanocrystals to the required location [108]. Alternatively, figure 4, illustrates how dip-pen nanolithography (DPN) enables the nano-positioning of solvent-dispersed CQDs. For instance, the technique has been used to position a single CdSe/CdS core/shell CQD of ∼20 nm diameter at the centre of a nano-antenna, resulting in an 85% collection efficiency of single photons [109].

The discussion so far has focused on the potential of doped CQDs as a platform that presents a 'material vacuum' to the single spin qubit they host i.e., they effectively isolate the qubit form extraneous spins. However, there are circumstances where it might be beneficial to allow the qubit to couple to another spin. As mentioned above, this could be a nuclear spin (either on the same atom as the electronic spin, or on a

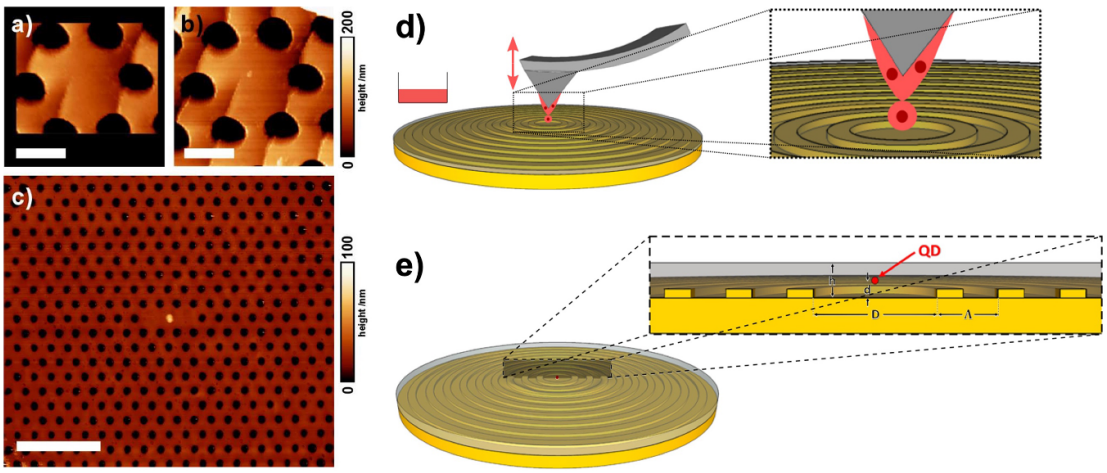

Figure 4. A photonic crystal fibre before (a) and after (b) the placement of a nanodiamond using an AFM tip. (c) A GaP photonic crystal membrane cavity with a nanodiamond positioned in its centre. Scale bars are 1 μm. Reproduced from [108], with the permission of AIP Publishing. This figure has been adapted from the original publication. Schematics of (d) the placement of CdSe/CdS core/shell CQD at the centre of a nanoantenna using DPN and (e) the location of the CQD after positioning. Reproduced from [109]. CC BY 4.0.

proximal atom) to act as a longer term quantum memory, or to a similar spin qubit in an adjacent CQD and thereby create entanglement for use in quantum information processing [10]. In the latter case, the spacing between the dopants will be critical but established techniques of CQD synthesis and assembly allow precise control of this separation. CQD can self-assemble to close packed arrays, forming a 'superlattice' [110]. For single dopants localised within the CQD cores, the separation between one dopant and its neighbours will be determined by the CQD size, shell thickness (if it has one) and the CQD packing density, with this latter parameter controlled by the organic surface ligands used. However, any design that allows such spin coupling between adjacent CQDs may also expose the spin qubits to uncontrolled spins on the CQD surface, and thereby compromise the coherence lifetime of that spin.

3.4. Comparison with NV centres in nanodiamonds

The NV centre in nanodiamonds is a solid-state spin-photon interface that has been comprehensively studied for applications in quantum technology and is thus a useful comparator for singly doped CQDs. As shown in table 1, its spin coherence lifetime has been reported to be 400 μs and so significantly longer than the lifetime reported for core-only Mn^{2+}:PbS CQDs although, as discussed above, there is scope to improve this considerably via a core–shell architecture and the use of a CQD composition using spin-0 atoms.

For a spin-photon interface, the optical properties are also important, determining the rate and efficiency at which spin states can be successfully prepared and read out; the timescales over which these processes can be achieved should be shorter than the spin coherence lifetime. The optical absorption cross-section for NV nanodiamonds of 40 nm size is on average about [111] 5×10^{-17} cm^2, whereas for CQDs the cross-section for a band edge exciton can be up to [98] $\sim 1 \times 10^{-15}$ cm^2; this implies that it will take significantly fewer attempts to write a spin state to a CQD using single photons than to a nanodiamond, all other factors being equal. The PL QY can vary significantly between NV nanodiamonds with values ranging between 5% and 20% reported [111] whilst QY $\sim$ 100% can be achieved for CQDs ensembles, which implies that the individual CQDs all have the same QY [11, 112]. NV nanodiamonds have excellent photostability [113] and whilst core-only CQDs typically suffer from PL intermittency (known as 'blinking') well-engineered core/shell CQDs can exhibit photostability and be blinking-free [112]._The radiative lifetime, τ_r, for NV nanodiamonds can be estimated from the PL lifetime τ_{PL},via $\tau_r = \tau_{PL}, /QY$, which for $\tau_{PL} \sim 10$ ns [114] and QY $\sim$ 10% [111] yields $\tau_r \sim 100$ ns. In comparison, τ_r for CQDs depends on their size, composition and structure but are typically 10–100 ns [10] and so broadly similar to NV nanodiamonds. NV nanodiamonds emit in the red part of the spectrum with a bandwidth that is $\sim$100 nm broad at room temperature, with only 4% being emitted into the zero-phonon line (ZPL) at room temperature [115] so that cryogenic temperatures are required for higher production rates of the indistinguishable photons needed for quantum technologies such as quantum repeaters. For single CQDs, the PL wavelength is size—and composition tunable and at 4 K the emission can be largely from the ZPL, with a sub-meV peak width [116]. Thus, whilst NV centres in nanodiamonds currently exhibit longer spin coherence lifetimes than doped CQDs, this must be balanced against the more favourably optical properties, particularly the significantly greater absorption

cross-section and PL QY of CQDs, which reduce the time needed to optically write, readout and entangle qubits. Moreover, the precise synthetic control that has been developed for CQDs over three decades that has resulted in these excellent optical properties also promises to be able to significantly increase the spin coherence lifetime in singly doped CQDs.

4. Next steps

As described above, singly doped CQDs are a promising platform for optically addressable spin qubits. The precise control over composition, size, and structure now available after more than three decades of synthetic development offers an exciting opportunity to optimise the optical, electronic and spin properties of a semiconductor nanostructure for applications in quantum technology. CQDs are large enough to be manipulated with an AFM tip but small enough to couple efficiently to the quantum properties of individual dopant atoms providing, via a photonic structure such as micro-cavity, an effective link between size-scales. Drawing on the closely related field of doped self-assembled quantum dots, a good understanding of the interaction between dopant and exciton exists, particularly for the well-studied Mn^{2+} dopant.

However, there are number of outstanding questions that remain and research directions that are not yet fully explored. For instance, it has not yet been established to what degree the nuclear spins of the core affect the spin coherence lifetime of the dopant. Another challenge is to confirm whether it is possible to purposefully couple electronic to nuclear spins in CQDs as a means of achieving much longer-term storage times of spin state. This has been demonstrated for self-assembled quantum dots but is un-explored for CQDs. Also, described in more detail below, much of the work reported so far on doped-CQDs has concentrated on Mn^{2+}, with other dopants much less studied. Rare earth dopants are intriguing possibilities, offering long spin coherence lifetimes and emission at telecoms wavelengths, but is not clear if they can be coupled efficiently to the band edge exciton.

In the following section, some next steps are suggested which will both enable some of these questions to answered and also further develop doped CQDs as a practical platform for quantum technology.

4.1. Reliable single atom doping

Most of the doping techniques developed so far are probabilistic in nature; controlling the concentration of the dopant species used in the synthesis process only determines the average doping in an ensemble of CQDs [21], with the probability of an individual CQD incorporating one or more dopants being described by a Poissonian distribution. Moreover, the position of the dopant within the CQD produced by these methods is also random, leading to significant variation in the exchange interaction between dopant and exciton [24] and coupling to surface spins [91]. This variation could necessitate the characterisation of a large number of CQDs individually before one is found with the required properties for incorporation into a device structure. Ideally, CQDs would be produced that were reliably doped with a single atom in the central region of each CQD.

Ensuring that doping is only within the central region of the CQD can be achieved by growing a doped core and growing an undoped shell of the same material around it [91]. This not only isolates the dopant from any spins on the surface, as demonstrated previously [91], but also ensures that the dopant is located in a region of the CQD where the exciton wavefunction, $\boldsymbol{\Psi}_{\boldsymbol{e}}(\boldsymbol{R})$ has close to its maximum magnitude and so produces a significant exchange interaction between exciton and dopant, as discussed in section 2.3. Optimising the doping level such that the average number of dopants per CQD is $\sim$1 will ensure that $\sim$37% of individual CQDs will contain one and only one dopant, assuming a Poissonian distribution. Finding a singly doped CQD from such as a distribution, using the characteristic PL signature shown in figure 3(c) as a selection criterion, thus becomes practical.

4.2. Extending the library of single dopants

Although a wide range of different atoms have been studied as dopants, this has been predominantly for the case of when there are multiple dopants per CQD [21]. In contrast, reports on singly doped CQDs have overwhelmingly concentrated on Mn^{2+} as the dopant. Expanding the number of different single dopants available would increase the utility of the singly doped CQDs. Potential advantages of alternate dopants include longer spin coherence lifetimes and emission at telecommunications wavelengths.

Among other TM dopants, Kobak *et al* [117] proposed Fe^{3+} as a promising candidate since the rate of spin relaxation increases with the strength of the spin–orbit interaction and Fe^{3+}, like Mn^{2+}, has zero orbital angular momentum. Moreover, unlike Mn, there are stable spin-0 isotopes of Fe (in fact 98% of naturally occurring Fe is composed of such isotopes). Cu^{2+} also has weak spin–orbit interaction due to its low electronic spin of $S = 1/2$, which also brings the benefit of a two-level fine structure corresponding to a simple qubit. However, Cu has no stable spin-0 isotopes and so the electronic spin cannot be decoupled from

nuclear spin by isotope selection. Spin coherence lifetime is also reduced by the spin–orbit interaction with the host material [117], but this is weaker for light anions indicating that sulphide- and phosphide-based host materials are preferable. In order to also remain isovalent with the dopant, this suggests combinations such as Cu^{2+}:ZnS and Fe^{3+}:InP.

The TM ions discussed above typically emit at wavelengths <900 nm [99], whereas for maximum propagation distances along optical fibres a wavelength of ∼1.5 μm is required. In contrast, lanthanide ion dopants offer a wide range of possible optical transitions spanning the visible to the infrared and most contain one or more unpaired *f*-shell electrons that could be used as a spin qubit. In particular, the $^4I_{15/2}$ to $^4I_{13/2}$ transition in Er^{3+} corresponds to emission in this band and is used to dope fibre amplifiers in telecoms system. This is a *f*–*f* transition and so optically created spins in these states are largely isolated from the environment, increasing their lifetime. However, these transitions also have low absorption cross-sections making steps such as the use optical micro-cavities which increase the probability of a successful interaction attempt with a single photon even more important. Finding a suitable CQD host material is more challenging for RE ions (Ln^{3+}) since they are typically hard Lewis acids, requiring a co-ordination number of six or more, whereas many CQD materials have a co-ordination number of four [118]; the substitution site must be large to accommodate the Ln^{3+} ion; and charge balance must be maintained after substitution. CQDs based on halide perovskites, $CsPbX_3$ (X = Cl, Br, or I), have great potential as the host for Ln^{3+} dopants because their optical properties are remarkably defect tolerant and are minimally affected by the introduction of impurities [118]. Moreover, they contain an octahedral site that is large enough to contain Pb^{2+}, which can be successfully substituted for Ln^{3+}. However, this creates a charge mismatch, which is likely to be compensated by a defect [118] that may host an unwanted spin. Another intriguing possibility is to use a RE compound as the host material and to dope it with another RE. For instance, the synthesis of CQDs based on lanthanide oxysulphides, Ln_2SO_2, has been reported, in which multiple RE ions have been incorporated into each CQD by mixing precursors for each prior to their thermolysis [119]. In this way, the coordination number, ionic radius and ion charge of the dopant are all well matched to the host.

5. Summary

There are several materials systems currently being investigated as the platform for optically addressed spin-qubits, including nitrogen vacancies in diamond [82] and RE-doped crystals such as yttrium orthosilicate [87]. It is not yet clear which material platform or platforms will be eventually adopted as the basis for the photon-spin interfaces that will be used in quantum technologies such as quantum memories. In this perspective, we argue that singly doped CQDs have a combination of key properties that make them particularly well-suited as photon-spin interfaces, competitive with more well-studied platforms.

Firstly, CQDs offer a material vacuum for the dopant i.e. a local environment that is free of the extraneous spins that would otherwise reduce the spin coherence lifetime. CQDs are subject to 'self-purification' process by which defects, and the spins associated with them, are expelled from the volume of the CQD. A dopant localised to the central region of the CQD can be isolated from the spins on the surface or the immediate vicinity by a thick graded-composition shell layer that can be grown round the dopant-containing core. Further, nuclear spins can also be avoided by using isotopically selected precursors. Secondly, the typically weak optical interaction cross-section of single dopants can be enhanced by orders of magnitude by size-tuning the bandgap of the CQD so that the dopant fine structure couples with the band edge exciton. Thirdly, CQDs are isolated nanocrystals, free of any substrate, of a few nm to a few 10 s of nm in size, which means that an individual CQD and the single spin qubit it contains can be manipulated with an AFM tip or via DPN and placed within a micro-cavity of other photonic structure to further enhance the photon-spin coupling. Lastly, CQDs benefit from a well-established suite of synthetic and processing synthetic techniques, and proven scalability and compatibility with large scale manufacturing.

We have also identified two areas for further development in synthetic methods that would significantly improve the impact of singly doped CQDs as photon-spin interfaces. The first of these is deterministic doping of the CQDs so that, to a high yield, each is doped by one and only one dopant and that dopant is in the centre of the CQD. The other area of development is to extend the library of elements that can be incorporated as single dopants in CQDs. Amongst the TMs, Fe^{3+} and Cu^{2+} promise to have weak spin–orbit interactions and hence longer spin coherence lifetimes, and these can be combined with established CQD composition such as InP and ZnS with light anions, which further reduce the spin–orbit interaction. Of the REs, Er^{3+} is of particular interest because its emission band corresponds to the wavelength used for fibre-based telecommunications. Finding a suitable CQD composition is more challenging for RE dopants because of their high co-ordination number, large ionic radius and oxidation state, but promising materials are in development, such as the oxysulphides of other REs.

Data availability statement

No new data were created or analysed in this study.

Acknowledgments

This work was supported by funding from UKRI Innovate UK (Grant No. TS/X002195/1). Both authors contributed equally to the writing. No new data was generated and there are no conflicts of interest to declare.

ORCID iD

David J Binks https://orcid.org/0000-0002-9102-0941

References

[1] Rossetti R, Nakahara S and Brus L E 1983 *J. Chem. Phys.* **79** 1086–8
[2] Ekimov A I, Efros A L and Onushchenko A A 1985 *Solid State Commun.* **56** 921–4
[3] Efros A L and Brus L E 2021 *ACS Nano* **15** 6192–210
[4] Nozik A J 2002 *Physica* E **14** 115–20
[5] Konstantatos G, Howard I, Fischer A, Hoogland S, Clifford J, Klem E, Levina L and Sargent E H 2006 *Nature* **442** 180–3
[6] Coe S, Woo W-K, Bawendi M and Bulovic V 2002 *Nature* **420** 800–3
[7] Vandyshev Y, Dneprovskii V, Klimov V and Okorokov D 1991 *JETP Lett.* **54** 441–4 (available at: http://jetpletters.ru/ps/1251/article_18924.pdf)
[8] Martynenko I V, Litvin A P, Purcell-Milton F, Baranov A V, Fedorov A V and Gun'ko Y K 2017 *J. Mater. Chem.* B **5** 6701–27
[9] Panfil Y E, Oded M and Banin U 2018 *Angew. Chem., Int. Ed.* **57** 4274–95
[10] Kagan C R, Bassett L C, Murray C B and Thompson S M 2021 *Chem. Rev.* **121** 3186–233
[11] Page R *et al* 2015 *Small* **11** 1548–54
[12] Michler P, Imamoglu A, Mason M D, Carson P J, Strouse G F and Buratto S K 2000 *Nature* **406** 968–70
[13] Ihara T, Miki S, Yamada T, Kaji T, Otomo A, Hosako I and Terai H 2019 *Sci. Rep.* **9** 15941
[14] Lin X, Dai X, Pu C, Deng Y, Niu Y, Tong L, Fang W, Jin Y and Peng X 2017 *Nat. Commun.* **8** 1132
[15] Bozyigit D, Yazdani N, Yarema M, Yarema O, Lin W M M, Volk S, Vuttivorakulchai K, Luisier M, Juranyi F and Wood J 2016 *Nature* **531** 618–22
[16] Empedocles S A and Bawendi M G 1999 *J. Phys. Chem.* B **103** 1826–30
[17] Ye M and Searson P C 2011 *Phys. Rev.* B **84** 125317
[18] Utzat H *et al* 2019 *Science* **363** 1068–72
[19] Hu H and Zhang W 2006 *Opt. Mater.* **28** 536–50
[20] Liu M, Yazdani N, Yarema M, Jansen M, Wood V and Sargent E H 2021 *Nat. Electron.* **4** 548–58
[21] Erwin S C, Zu L, Haftel M I, Efros A L, Kennedy T A and Norris D J 2005 *Nature* **436** 91–94
[22] Shao H, Wang C, Xu S, Jiang Y, Shao Y, Bo F, Wang Z and Cui Y 2014 *Nanotechnology* **25** 025603
[23] Kagan C R and Murray C B 2015 *Nat. Nanotechnol.* **10** 1013
[24] Fainblat R, Barrows C J and Gamelin D R 2017 *Chem. Mater.* **29** 8023–36
[25] Fainblat R, Barrows C J, Hopmann E, Siebeneicher S, Vlaskin V A, Gamelin D R and Bacher G 2016 *Nano Lett.* **16** 6371–7
[26] Awschalom D D, Hanson R, Wrachtrup J and Zhou B B 2018 *Nat. Photon.* **12** 516–27
[27] Kruis F E, Fissan H and Peled A 1998 *J. Aerosol Sci.* **29** 511–35
[28] Kruis F E, Goossens A and Fissan H 1996 *J. Aerosol Sci.* **27** 165–6
[29] Gresback R, Hue R, Gladfelter W L and Kortshagen U R 2011 *Nanoscale Res. Lett.* **6** 68
[30] Wu C-L and Zhao Y-B 2007 *Anal. Bioanal. Chem.* **388** 717–22
[31] Evans C M, Cass L C, Knowles K E, Tice D B, Chang R P H and Weiss E A 2012 *J. Coord. Chem.* **65** 2391–414
[32] Li C, Hassan A, Palmai M, Snee P T, Baveye P C and Darnault J G 2020 *J. Nanoparticle Res.* **22** 349
[33] Byun H-J, Lee J C and Yang H 2011 *J. Colloid Interface Sci.* **355** 35–41
[34] Murray C B, Norris D J and Bawendi M G 1993 *J. Am. Chem. Soc.* **115** 8706–15
[35] Abe S, Čapek R K, de Geyter B and Hens Z 2012 *ACS Nano* **6** 42–53
[36] Dadyburjor D B and Ruckenstein E 1977 *J. Cryst. Growth* **40** 279–90
[37] Jones M, Lo S S and Scholes G D 2009 *Proc. Natl Acad. Sci.* **106** 3011–6
[38] Eijt S W H, van Veen A, Schut H, Mijnarends P E, Denison A B, Barbiellini B and Bansil A 2006 *Nat. Mater.* **5** 23–26
[39] Ladd C, So J-H, Muth J and Dickey M D 2013 *Adv. Mater.* **25** 4953–5114
[40] Carter A C, Bouldin C E, Kemner K M, Bell M I, Woicik J C and Majetich S A 1997 *Phys. Rev.* B **55** 13822
[41] Biadala L *et al* 2017 *Nat. Nanotechnol.* **12** 569–74
[42] Rodina A V, Golovatenko A A, Shornikova E V, Yakovlev D R and Efros A L 2018 *Semiconductors* **52** 572–4
[43] Li J J, Wang A, Guo W, Keay J C, Mishima T D, Johnson M B and Peng X 2003 *J. Am. Chem. Soc.* **125** 12567–75
[44] Zaini M S, Liew J Y C, Ahmad S A A, Mohmad A R and Kamarudin M A 2020 *Appl. Sci.* **10** 6282
[45] Shen H, Lin Q, Cao W, Yang C, Shewmon N T, Wang H, Niu J, Li L S and Xue J 2017 *Nanoscale* **9** 13583
[46] Smith A M and Nie S 2010 *Acc. Chem. Res.* **43** 190–200
[47] Yang Y, Zheng Y, Cao W, Titov A, Hyvonen J, Manders J R, Xue J, Holloway P H and Qian L 2015 *Nat. Photon.* **9** 259–66
[48] Xie R, Kolb U, Li J, Basché T and Mews A 2005 *J. Am. Chem. Soc.* **127** 7480–8
[49] Panda S K, Hickey S G, Demir H V and Eychmuller A 2011 *Angew. Chem., Int. Ed.* **50** 4432–43
[50] Mocatta D, Cohen G, Schattner J, Millo O, Rabani E and Banin U 2011 *Science* **332** 77–81
[51] Chen D, Viswanatha R, Ong G L, Xie R, Balasubramaninan M and Peng X 2009 *J. Am. Chem. Soc.* **131** 9333–9
[52] Dalpian G M and Chelikowsky J R 2006 *Phys. Rev. Lett.* **96** 226802
[53] Norris D J and Bawendi M G 1996 *Phys. Rev.* B **53** 16338–46

[54] Beaulac R, Feng Y, May J W, Badaeva E, Gamelin D R and Li X 2011 *Phys. Rev.* B **84** 195324
[55] Beaulac R, Schneider L, Archer P I, Bacher G and Gamelin D R 2009 *Science* **325** 973–6
[56] Hoffman D M, Meyer B K, Ekimov A I, Merkulov A, Efros A L, Rosen M, Couino G, Gacoin T and Boilot J P 2000 *Solid State Commun.* **114** 547–550
[57] Bussian D, Crooker S, Yin M, Brynda M, Efros A L and Klimov V I 2009 *Nat. Mater.* **8** 35–40
[58] Pandey A, Brovelli S, Viswanatha R, Li L, Pietryga J M, Klimov V I and Crooker S A 2012 *Nat. Nanotechnol.* **7** 792–7
[59] Archer P I, Santangelo S A and Gamelin D R 2007 *Nano Lett.* **4** 1037–43
[60] Besombes L, Boukari H, Tiwari V, Lafuente-Sampietro A, Kuroda S and Makita K 2019 *Semicond. Sci. Technol.* **34** 063001
[61] Lafuente-Sampietro A, Boukari H and Besombes L 2015 *Phys. Rev.* B **92** 081305
[62] Lee D, Lee K W, Cady J V, Ovartchaiyapong P and Bleszynski Jayich A C 2017 *J. Opt.* **19** 033001
[63] Moro F, Turyanska L, Granwehr J and Patanè A 2014 *Phys. Rev.* B **90** 205428
[64] Borse P H, Srinivas D, Shinde R F, Date S K, Vogel W and Kulkarni S K 1999 *Phys. Rev.* B **60** 8659
[65] Clerjaud B and Gélineau A 1977 *Phys. Rev.* B **16** 82
[66] Vlaskin V A, Beaulac R and Gamelin D R 2009 *Nano Lett.* **9** 12 4376–4382
[67] Gaj J A, Planel R and Fishman G 1979 *Solid State Commun.* **29** 435–8
[68] Norris D J, Yao N, Charnock F T and Kennedy T A 2001 *Nano Lett.* **1** 3–7
[69] Bradshaw L R, May J W, Dempsey J L, Li X and Gamelin D R 2014 *Phys. Rev.* B **89** 115312
[70] Ochsenbein S T, Feng Y, Whitaker K M, Badaeva E, Liu W K, Li X and Gamelin D R 2009 *Nat. Nanotechnol.* **4** 681–7
[71] Abolfath R M, Hawrylak P and Žutic I 2007 *Phys. Rev. Lett.* **98** 207203
[72] Hoffmann A and Bader S D 2015 *Phys. Rev. Appl.* **4** 047001
[73] Bhattacharjee A K and Benoit`a la Guillaume C 1997 *Phys. Rev.* B **55** 10613
[74] Shirasaki Y, Supran G J, Bawendi M G and Bulović V 2013 *Nat. Photon.* **7** 13–23
[75] Besombes L, Leger Y, Bernos J, Boukari H, Mariette H, Poizat J P, Clement T, Fernández-Rossier J and Aguado R 2008 *Phys. Rev.* B **78** 125324
[76] Le Gall C, Kolodka R S, Cao C L, Boukari H, Mariette H, Fernández-Rossier J and Besombes L 2010 *Phys. Rev.* B **81** 245315
[77] Govorov A O and Kalameitsev A V 2005 *Phys. Rev.* B **71** 035338
[78] Reiter D E, Kuhn T and Axt V M 2009 *Phys. Rev. Lett.* **102** 177403
[79] Muckel F, Barrows C J, Graf A, Schmitz A, Erickson C S, Gamelin D R and Bacher G 2017 *Nano Lett.* **17** 4768–73
[80] Léger Y, Besombes L, Fernández-Rossier J, Maingault L and Mariette H 2006 *Phys. Rev. Lett.* **97** 107401
[81] Moro F, Turyanska L, Wilman J, Fielding A J, Fay M W, Granwehr J and Patanè A 2015 *Sci. Rep.* **5** 10855
[82] Wood B D *et al* 2022 *Phys. Rev.* B **105** 205401
[83] Bernien H *et al* 2013 *Nature* **497** 86–90
[84] Sukachev D D, Sipahigil A, Nguyen C T, Bhaskar M K, Evans R E, Jelezko F and Lukin M D 2017 *Phys. Rev. Lett.* **119** 223602
[85] Stockill R, Gall C L, Matthiesen C, Huthmacher L, Clarke E, Hugues M and Atatüre M 2016 *Nat. Commun.* **7** 12745
[86] Nagy R *et al* 2019 *Nat. Commun.* **10** 1954
[87] Raha M, Chen S, Phenicie C M, Ourari S, Dibos A M and Thompson J D 2020 *Nat. Commun.* **11** 1605
[88] Norris D J, Efros A L and Erwin S C 2008 *Science* **319** 1776–9
[89] Pietryga J M, Park Y-S, Lim J, Fidler A F, Bae W K, Brovelli S and Klimov V I 2016 *Chem. Rev.* **116** 10513–622
[90] Jang E, Jun S and Pu L 2003 *Chem. Commun.* 2964–5
[91] Schimpf A M, Ochsenbein S T and Gamelin D R 2015 *J. Phys. Chem. Lett.* **6** 457–63
[92] Maurer P C *et al* 2012 *Science* **336** 1283
[93] Henglein A and Gutierrez M 1983 *Ber. Bunsenges.* **87** 852–8
[94] Zhong T *et al* 2018 *Phys. Rev. Lett.* **121** 183603
[95] Dibos A M, Raha M, Phenicie C M and Thompson J D 2018 *Phys. Rev. Lett.* **120** 243601
[96] Besombes L, Léger Y, Maingault L, Ferrand D, Mariette H and Cibert J 2004 *Phys. Rev. Lett.* **93** 207403
[97] Goryca M, Koperski M, Wojnar P, Smoleński T, Kazimierczuk T, Golnik A and Kossacki P 2014 *Phys. Rev. Lett.* **113** 227202
[98] Shim M and Philippe Guyot-Sionnest P 1999 *J. Chem. Phys.* **111** 6955
[99] Bhargava R N, Gallagher D, Hong X and Nurmikko A 1994 *Phys. Rev. Lett.* **72** 416–9
[100] Shen Y and Takenari Goto T G 1997 *Jpn. J. Appl. Phys.* **36** 1648–50
[101] Chakraborty S, Mondal P, Makkar M, Moretti L, Cerullo G and Viswanatha R 2023 *Chem. Mater.* **35** 2146–54
[102] Viswanatha R, Pietryga J M, Klimov V I and Crooker S A 2011 *Phys. Rev. Lett.* **107** 067402
[103] Le Gall C, Besombes L, Boukari H, Kolodka R, Cibert J and Mariette H 2009 *Phys. Rev. Lett.* **102** 12
[104] Gangloff D A, Éthier-Majcher G, Lang C, Denning E V, Bodey J H, Jackson D M, Clarke E, Hugues M, le Gall C and Atatüre M 2019 *Science* **364** 62–66
[105] Gillard G, Clarke E and Chekhovich E A 2022 *Nat. Commun.* **13** 4048
[106] Chekhovich E A, Hopkinson M, Skolnick M S and Tartakovskii A I 2015 *Nat. Commun.* **6** 6348
[107] Yang J, Choi M K, Kim D-H and Hyeon T 2016 *Adv. Mater.* **28** 1176–207
[108] Schell A W, Kewes G, Tim Schröder T, Wolters J, Aichele T and Benson O 2011 *Rev. Sci. Instrum.* **82** 073709
[109] Abudayyeh H *et al* 2021 *APL Photonics* **6** 036109
[110] Murray C B, Kagan C R and Bawendi M G 2000 *Annu. Rev. Mater. Sci.* **30** 545–610
[111] Plakhotnik T and Aman H 2018 *Diam. Relat. Mater.* **82** 87–95
[112] Won Y-H, Cho O, Kim T, Chung D-Y, Kim T, Chung H, Jang H, Lee J, Kim D and Jang E 2019 *Nature* **575** 634–8
[113] Reineck P *et al* 2016 *Adv. Opt. Mater.* **4** 1549–57
[114] Capelli M *et al* 2022 *New J. Phys.* **24** 033053
[115] Bradac C, Gao W, Forneris J, Trusheim M E and Aharonovich I 2019 *Nat. Commun.* **10** 5625
[116] Berkinsky D B *et al* 2023 *ACS Nano* **17** 3598–609
[117] Kobak J *et al* 2014 *Nat. Commun.* **5** 3191
[118] Marin R and Jaque D 2021 *Chem. Rev.* **121** 1425–62
[119] Ward-O'Brien B, McNaughter P D, Cai R, Chattopadhyay A, Flitcroft J M, Smith C T, Binks D J, Skelton J M, Haigh S J and Lewis D J 2022 *Nano Lett.* **22** 8045–51